



Cite this: *Dalton Trans.*, 2024, **53**, 10544

Temperature-dependent excited states for detecting reversible phase transitions in 2D lead(II) iodide perovskites†

Mahboubah Jamshidi * and James M. Gardner *

Significant interest exists in water-tolerant 2D lead iodide perovskites owing to their stability and proven potential in photovoltaic and photonic applications. These materials have solid-state phase transitions that are accessible below 100 °C. Here, the study witnesses the multiple phase transitions of the last members of a series of organic–inorganic hybrid materials, $[(C_nH_{2n+1}NH_3)_2PbI_4]$, with even n as $n = 14, 16$, and 18 , once again. By employing temperature-dependent steady-state photoluminescence (PL) and temperature-dependent time-resolved photoluminescence (TRPL) spectroscopy in the temperature range of -18 to $+90$ °C and at -196 °C, we explore the thermal responses of these materials. The investigation reveals reversible phase transitions occurring between room temperature (RT) and elevated temperatures, impacting the optical properties and emitting colors of the perovskite compounds. The longer the alkyl chain, the higher the phase transition temperature, attributed to increased conformational disorder and enhanced perovskite symmetry. The decay constants for all compounds are very close in value, which confirms the underlying excited-state dynamics, pointing to contributions primarily from inorganic components across different phases. We anticipate that our results on the detection of phase transitions in 2D perovskites will not only motivate the use of these techniques for detecting phase transitions but also would help to understand their excited states in more details to selectively use them for solar cell and next-generation display technologies.

Received 24th April 2024,
Accepted 23rd May 2024

DOI: 10.1039/d4dt01210k

rsc.li/dalton

1. Introduction

Two-dimensional (2D) lead halide perovskite semiconductors are a class of materials that have recently found applications in solar cells, light-emitting diodes, and photodetector technologies.¹ Although 3D perovskites, such as $CH_3NH_3PbI_3$, could be transformative for optoelectronic applications, they are presently limited by their chemical and thermal stability. Alternatively, 2D perovskites may be more promising for their incorporation in practical devices due to their long, hydrophobic alkyl chain cations.^{2–4} The general formula of these organic–inorganic hybrids is $(R-NH_3)_2PbX_4$ where R is a long-chain alkylammonium cation, and X is a halide. These perovskites consist of two-dimensional sheets of the corner-sharing octahedral anions $[PbX_6]^{4-}$ capped with alternating double layers of cations $(C_nH_{2n+1}NH_3)^+$, which are stabilized by hydro-

gen bonding between ammonium cations and halides in the inorganic layers.⁵

The layered structure creates a quantum well structure with strong electronic confinement effects that separates the inorganic lead(II) halide sheets from the organic cation double layers.⁶ The dielectric and excitonic characteristics of 2D perovskites are associated with their quantum well arrangement and can be adjusted through the incorporation of different halide anions and by modifying the thickness of the inorganic layer.^{7–9} Various alkylammonium ligand-based cations have been investigated for use within the context of 2D perovskites.^{10–13} Typically, short-chain cations are employed in 2D perovskite structures to minimize the separation between quantum wells, thereby facilitating charge transfer.^{14,15} Conversely, larger organic cations increase this separation, impeding charge transport and consequently diminishing device efficiency.^{16,17}

Two-dimensional perovskite compounds can undergo solid-state phase transitions. The temperature for the phase transitions increases as the alkylammonium cation carbon chain length increases, as confirmed by differential scanning calorimetry (DSC), differential thermal analysis (DTA), Raman spectroscopy, and single-crystal X-ray diffraction.^{18–22} According to single-crystal X-ray diffraction, there are three changes involved in

Department of Chemistry, Division of Applied Physical Chemistry, KTH Royal Institute of Technology, SE-100 44 Stockholm, Sweden. E-mail: mahjam@kth.se, jgardner@kth.se

† Electronic supplementary information (ESI) available: Experimental methods, global fitting parameters, relative quantum yields, and additional results of PL and decay constant measurements. See DOI: <https://doi.org/10.1039/d4dt01210k>



the phase transitions, which may occur independently or cooperatively in each phase transition.^{23,24} As the temperature increases, the Pb–X–Pb angle increases and results in lead(II) halide layers becoming more co-planar and the planes shifting from a staggered geometry to an eclipsed geometry. Also, the shift of the organic cation layer relative to the inorganic layer causes the angle of the ammonium cations to change from obtuse to acute. Lastly, there are rotations around C–C bonds in the alkylammonium cations, which have less impact on the inorganic layer.^{18,25,26} The number of unique phases depends on the length of the organic chain, for instance, the number of unique phases for a 2D lead(II) iodide perovskite with an alkyl chain of $n = 11$ and 15 is three, while there are four phases for $n = 13$.³

Recently, we investigated the longest, even-numbered members of the series of organic–inorganic hybrid materials, $[(C_nH_{2n+1}NH_3)_2PbI_4]$, with $n = 14, 16$, and 18 for their use as water-tolerant perovskites in solar cells.² From the crystallographic data and DSC, these materials undergo two first-order phase transitions in the range from +45 to +100 °C from fluctuations in the thermal motion of the alkylammonium chains positioned between the layers (Fig. 1).^{27,28} At room temperature, the organic chains are interdigitated in a planar conformation and nearly perpendicular to the inorganic layers. By increasing the temperature, the disorder in the alkyl chains and interlayer spacing increases.^{18,29}

For optoelectronic devices utilizing perovskites, it is necessary to have a detailed photophysical understanding of the compounds. There are several reports on excited states, photoluminescence quantum yields, and responsiveness to external stimuli. For example, for $APbX_3$ perovskites such as $A = Cs^+$, $CH_3NH_3^+$, or $NH_2CHNH_2^+$ ^{30–33} and 2D perovskites such as $(C_4H_9NH_3)_2PbI_4$ and $(BDA)PbBr_4$.^{34–36} However, the current study aims to show how photophysical properties change as a function of temperature across phase transitions which have not been thoroughly investigated and warrant further study.

Herein, we studied the excited states of two-dimensional perovskites in the powder form by temperature-dependent time-resolved photoluminescence spectroscopy (at –196 °C and from –18 to 95 °C) to investigate their phase transitions and develop an in-depth understanding of the excited state behavior across phase transitions. Above –18 °C, the PL spectra of all the perovskites were fitted with multipeak Gaussian functions to determine the contributions of individual phases.

2. Experimental methods

The synthesis protocol of 2D perovskites given in ref. 2 and 27 is followed for the preparation of $(C_{14}H_{29}NH_3)_2PbI_4$, $(C_{16}H_{33}NH_3)_2PbI_4$, and $(C_{18}H_{37}NH_3)_2PbI_4$ 2D perovskites. For the diffuse reflectance spectroscopic measurements, an Avantes AvaSpec-2048 dual UV-vis spectrophotometer, equipped with an integrating sphere and an integrated light source, was used to record the absorption of powders. Photoluminescence measurements were carried out on a Fluorolog FL 3–22 spectrometer (Horiba Jobin Yvon, Longjumeau, France), equipped with a double excitation monochromator, a single emission monochromator (HR320) and an R928P PMT detector. A continuous xenon lamp (450 W) was used for steady state measurements. A Delta Diode ($\lambda_{ex} = 360$ nm) was employed as the pulsed source for time correlated single photon counting (TCSPC) lifetime acquisition. The absolute quantum yield (QY) was measured with a G8 integrating sphere (GMP), using $BaSO_4$ and pure solvents as blanks at 25 °C. Integrated emission intensity as a function of temperature was compared with the measured absolute QY at room temperature to calculate the relative quantum yield based on the fixed parameters and conditions. Measurements at –196 °C were performed in liquid N_2 . A Luma 40 heat exchan-

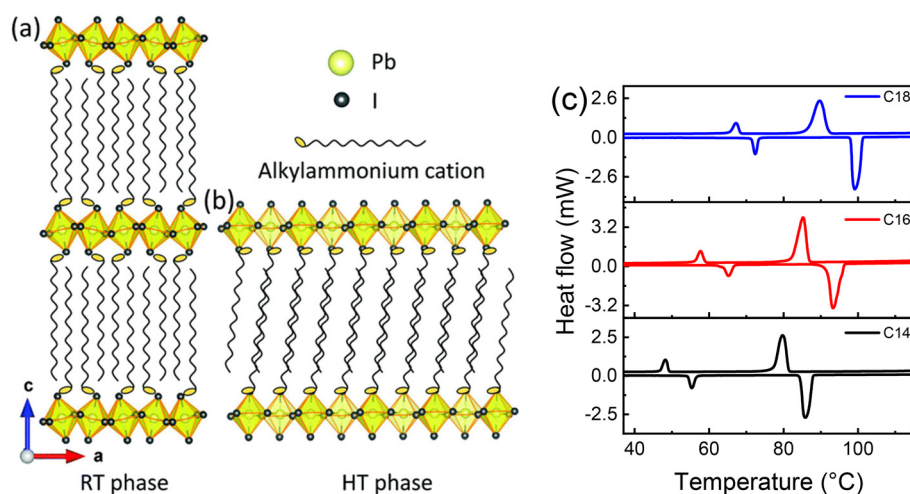


Fig. 1 The crystal structures of the $(C_{14}H_{29}NH_3)_2PbI_4$ perovskite (a) are orthorhombic at room temperature (RT) and (b) monoclinic at an elevated temperature (HT). The interdigitated arrangement of alkylammonium chains is shown as lines. The yellow spheres inside the polyhedra are Pb^{2+} cations and the black spheres are I^- anions. (c) DSC curves of the $(C_nH_{2n+1}NH_3)_2PbI_4$ ($n = 14, 16$ and 18) 2D perovskite powder samples measured in both heating and cooling cycles. Reprinted by permission from ref. 28.



ger connected to a TC 1 temperature controller filled with 50% methanol was used for temperature adjustment from -18 to 95 °C. A multi-exponential function was selected to fit PL decay curves:

$$I = \sum A_i \exp^{-t/\tau_i},$$

A_i is the pre-exponential factor and τ_i is the decay lifetime. High temperature data were fitted with the triple exponential decay equation and the lower temperature curves were fitted with the bi-exponential equation.

3. Results and discussion

The photoluminescence time constants, quantum yields, and emission maxima for $(C_nH_{2n+1}NH_3)_2PbI_4$ ($n = 14, 16$ and 18) powder samples are summarized in Table 1 and Table S1.†

The tables reflect the heating and cooling of the samples up to $+85$ °C and cooling to -18 and -196 °C.

The emission spectra of samples from room temperature to high temperature are similar to those in our previous report on the same samples but on thin film. The PL spectra reveal the presence of two resolved peaks in all three powder samples, which is complementary to the absorption results (Fig. S1†). The presence of two resolved peaks in the absorption and PL emission spectra could originate from the dual excitonic emission, vibronic coupling, simultaneous coexistence of the two crystallographic phases, or temperature-induced exciton switching in these compounds.^{37–42} The robust absorbance aligned with both PL peaks implies that neither of the two PL peaks stems from defect states. Typically, emissions linked to defects or traps lack the corresponding absorption, as localized defect states exhibit a notably low absorption cross-section.^{34,43}

Regarding the dual excitonic emission, there are some reports which could be seen in the single crystals of some 2D

Table 1 Emission maxima, time constants, pre-exponential factors, and quantum yields of $(C_nH_{2n+1}NH_3)_2PbI_4$ ($n = 14, 16$ and 18) powders at varied temperatures ($\lambda_{ex} = 360$ nm)

Compound	Temperature	λ_{em} (nm)	τ_{em} (ns) \pm standard error	A_i	Φ_{PL} [%]
$(C_{18}H_{37}NH_3)_2PbI_4$	85 °C	584	$\lambda_{det} = 578$ nm		0.08
			$\tau_1 = 53.3 \pm 0.9$	0.56	
			$\tau_2 = 261 \pm 4$	0.33	
			$\tau_3 = 1043 \pm 12$	0.12	
	25 °C	493, 523	$\lambda_{det} = 493$ nm		2.75
			$\tau_1 = 57 \pm 1$	0.60	
			$\tau_2 = 272 \pm 5$	0.30	
			$\tau_3 = 1095 \pm 17$	0.10	
			$\lambda_{det} = 523$ nm		
			$\tau_1 = 59 \pm 3$	0.60	
	−10 °C	490, 507	$\tau_2 = 297 \pm 19$	0.30	3.06
			$\tau_3 = 1253 \pm 85$	0.10	
			$\lambda_{det} = 490$ nm		
			$\tau_1 = 50 \pm 2$	0.72	
$(C_{16}H_{33}NH_3)_2PbI_4$	−196 °C	484	$\tau_2 = 270 \pm 17$	0.22	
			$\tau_3 = 1200 \pm 70$	0.06	
			$\lambda_{det} = 484$ nm		
			$\tau_1 = 42 \pm 4$	0.90	
	25 °C	498, 536	$\tau_2 = 394 \pm 28$	0.10	0.27
			$\lambda_{det} = 498$ nm		
			$\tau_1 = 42 \pm 1$	0.67	
			$\tau_2 = 241 \pm 6$	0.25	
			$\tau_3 = 1081 \pm 25$	0.08	
			$\lambda_{det} = 536$ nm		
	−196 °C	483, 645	$\tau_1 = 54 \pm 1$	0.58	
			$\tau_2 = 260 \pm 5$	0.31	
			$\tau_3 = 1041 \pm 15$	0.11	
			$\lambda_{det} = 498$ nm		
$(C_{14}H_{29}NH_3)_2PbI_4$	25 °C	495, 525	$\tau_1 = 39 \pm 1$	0.85	1.45
			$\tau_2 = 385 \pm 8$	0.15	
			$\lambda_{det} = 495$ nm		
			$\tau_1 = 28 \pm 2$	0.80	
			$\tau_2 = 184 \pm 9$	0.15	
			$\tau_3 = 931 \pm 36$	0.05	
	−196 °C	485	$\lambda_{det} = 525$ nm	0.05	
			$\tau_1 = 53 \pm 2$	0.60	
			$\tau_2 = 265 \pm 8$	0.30	
			$\tau_3 = 1093 \pm 29$	0.10	
			$\lambda_{det} = 485$ nm		
			$\tau_1 = 37 \pm 3$	0.79	
			$\tau_2 = 234 \pm 12$	0.16	
			$\tau_3 = 1125 \pm 57$	0.05	



perovskites such as $(\text{C}_4\text{H}_9\text{NH}_3)_2\text{PbI}_4$,⁴⁰ $(\text{C}_8\text{H}_{17}\text{NH}_3)_2\text{PbI}_4$,⁴⁴ and A_2SnI_4 (with A = phenylethylammonium, butylammonium, hexylammonium, and octylammonium monovalent cations).³⁷ However, herein we believe that the dual peaks are coming from two different phases. To further confirm the origin of the peaks and confirm the existence of two phases, we have measured the PL emission spectra of the freshly prepared

powder samples that were not annealed (Fig. S2†). The PL emission peak at a shorter wavelength exactly overlaps with the PL emission spectra recorded in the fresh powder samples, indicating that the peak at longer wavelengths results from the presence of the HT phase. It suggests that the RT phase is the product which takes time to be converted partially to the HT phase at room temperature without annealing. This is further

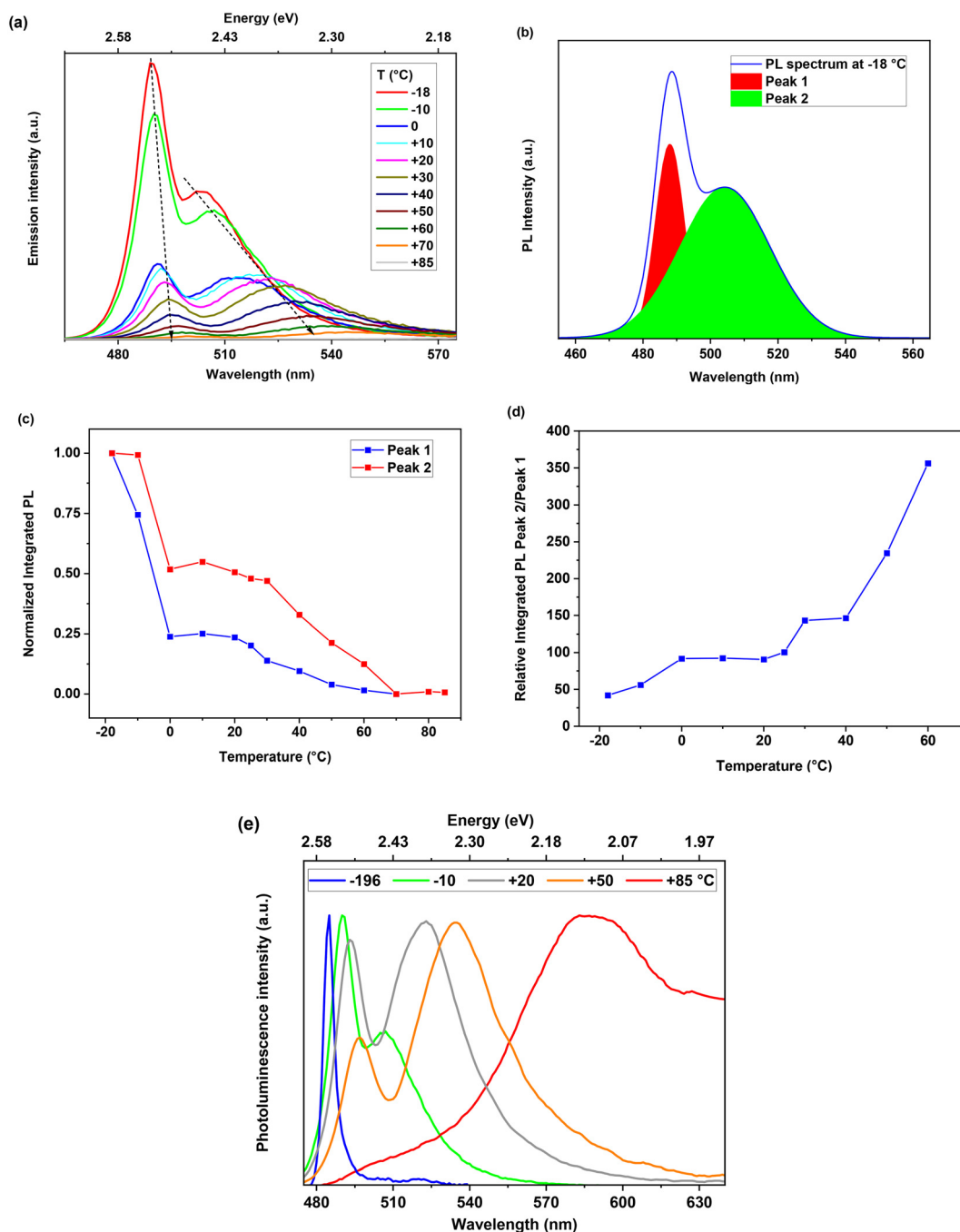


Fig. 2 (a) Temperature-dependent photoluminescence spectra of $(\text{C}_{18}\text{H}_{37}\text{NH}_3)_2\text{PbI}_4$. (b) Fitting of PL spectra with a multi-peak Gaussian function at -18 °C. (c) Variation of integrated PL intensity emission peak maxima of $(\text{C}_{18}\text{H}_{37}\text{NH}_3)_2\text{PbI}_4$ in the temperature range from -18 to 85 °C with $\lambda_{\text{ex}} = 360$ nm. (d) Comparison of the relative integrated intensities of the low energy (Peak 2) to high energy peak (Peak 1) in percentages. (e) Normalized photoluminescence spectra of $(\text{C}_{18}\text{H}_{37}\text{NH}_3)_2\text{PbI}_4$ from -196 °C to 85 °C.



demonstrated by PXRD, wherein the initial peak exhibits a shift over time (Fig. S3†).

In order to distinguish the influences originating from the emission states of different phases in the photoluminescence spectra, we utilized a Gaussian fitting function with multiple peaks to compare the photoluminescence spectra for temperatures between -18 and 85 °C. Starting the steady state measurements at -18 °C, a sharp emission peak (Peak 1) with the maximum intensity at 489 nm and a broad peak at 503 nm (Peak 2) were observed with a quantum yield of 6.3% (Fig. 2a and S8†). The population of the peaks at -18 °C was fitted using gaussian distributions as shown in Fig. 2b. The population of Peak 1 is lower than that of Peak 2 in this temperature range (Fig. 2d). Increasing the temperature leads to a bathochromic shift in Peak 1 and a pronounced bathochromic shift in Peak 2 (Fig. 2a) with a relatively broad emission bandwidth. At 0 °C, the integrated PL intensity of both peaks significantly decreased (Fig. 2c). The intensity remained relatively constant between 0 and 20 °C. The intensities gradually decreased with the increasing temperature and were quenched at 70 °C and 85 °C for Peak 1 and Peak 2, respectively.

The absolute quantum yield was measured as 2.75% at 20 °C (Fig. 2c). At temperatures above 20 °C, the intensities diminished and at 85 °C, only Peak 2 (584 nm) was observed and quantum yield reduced significantly to 0.06% compared to room temperature (Fig. 2e and S8†). Finally, the emission is quenched below the detection limit at 90 °C, which is consistent with the reported phase transition temperature for $(\text{C}_{18}\text{H}_{37}\text{NH}_3)_2\text{PbI}_4$ (Fig. 1c).^{18,28}

It is noteworthy to mention that the quenching of the emission is accompanied by the emergence of a higher temperature phase due to annealing the sample to 100 °C.²⁸ When viewed under ambient light, the color of the sample is yellow below the phase transition temperature, but it is orange at 80 °C

(Fig. 3a and b). Additionally, the bright green emission from UV excitation at ambient temperature is quenched at 85 °C (Fig. 3c) and above as non-emissive phase dominates at higher temperatures.

The inverse temperature response is observed upon cooling the same sample from 85 to -18 °C, which confirms the reversibility of the phase transition (Fig. S4†).

At -196 °C (77 K) there is a sharp, narrow photoluminescence peak (Peak 1) at 483 nm, which is hypsochromically shifted at ~ 420 cm^{-1} compared to room temperature (493 nm), as shown in Fig. 2e. We speculate that dual emission comes from the co-existence of the room temperature phase and the high temperature phase (Peak 2, orthorhombic structure). If the peaks were originated from the same phase, then the vibronic structure of the emission would have sharp, distinct peaks, which was not observed. The stability of the compounds was confirmed by comparing the PL of a sample that was thermally cycled with that of a sample that was not. The spectra of the two samples are the same, which confirms the reversibility.

To gain further insights into the optical and physical transitions, variable temperature time-resolved photoluminescence (TRPL) measurements were performed. Herein, decay traces were fitted to multiexponential functions with short (<100 ns), medium (100–400 ns), and long (>400 ns) time constants.

As shown in Fig. 4a, the decay traces of the sample were recorded at two detection wavelengths that correspond to the two maxima in the PL spectra. At room temperature, the PL decay traces are fitted as a triple exponential decay process. The time constants for the traces at 493 nm and 523 nm are similar ($\tau_1 = 57$ vs. 59 ns, $\tau_2 = 272$ vs. 297 ns, and $\tau_3 = 1.09$ vs. 1.25 μs for $\lambda_{\text{det}} = 493$ nm and 523 nm, respectively) and suggesting that they are produced by the same process or that there is mixing between the two excited states. The pre-exponential factors show consistent contributions at both PL maxima ($A_1 = 0.6$, $A_2 = 0.3$, and $A_3 = 0.10$). In addition, the same decay dynamics in the emission wavelengths suggest that these two bands are not caused by defect states, which could present different decay dynamics.⁴⁰

Based on the time constants, we posit that the emission of Peak 2 originates from the inorganic ordered sublattice singlet state and triplet states in the orthorhombic structure (RT phase). Excitation principally occurs within the inorganic quantum well singlet state; however, the perovskites have heavy ions (Pb^{2+} and I^-), which facilitate spin-orbit coupling between singlet and triplet states of the inorganic well.^{45,46} At 85 °C, all detected emissions come from Peak 2, which refers to the HT phase (Fig. 4a). Above 85 °C, the emission is quenched (Fig. 3a and b).

Measuring the time-resolved PL from the room temperature phase ($\lambda_{\text{det}} = 490$ nm) at -10 °C indicates that the time constants are similar to those at 25 °C ($\tau_1 = 50$ ns, $\tau_2 = 270$ ns, and $\tau_3 = 1.2$ μs), but the contribution of the shortest time constant increased, and the overall quantum yield increased to 3.06%. At -196 °C, only the narrow PL peak is observed (Peak 1), and the PL decay curve ($\lambda_{\text{det}} = 484$ nm) no longer includes the

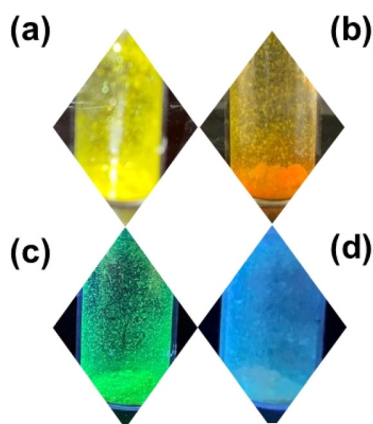


Fig. 3 Pictures of $(\text{C}_{18}\text{H}_{37}\text{NH}_3)_2\text{PbI}_4$ under ambient light at (a) 25 °C and (b) after heating the sample to 85 °C. Pictures of the same sample observed under UV illumination at (c) RT and (d) -196 °C (77 K). $(\text{C}_{18}\text{H}_{37}\text{NH}_3)_2\text{PbI}_4$ exhibits thermochromism, with the photoluminescence (PL) color changing from blue at -196 °C (77 K) to green at 25 °C (300 K).



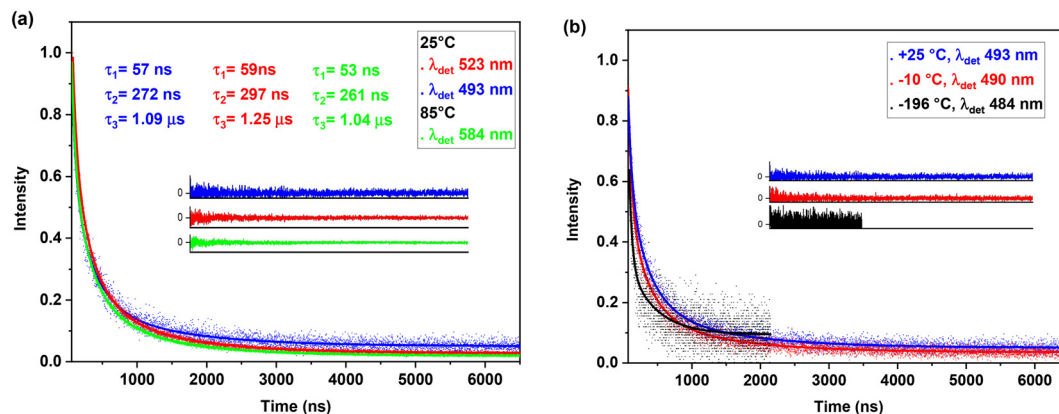


Fig. 4 Normalized time-resolved photoluminescence decay traces for $(\text{C}_{18}\text{H}_{37}\text{NH}_3)_2\text{PbI}_4$ powders at (a) room temperature at $\lambda_{\text{det}} = 493$ and 523 nm and at 85 °C at 584 nm, (b) 25, -10, and -196 °C for comparison ($\lambda_{\text{ex}} = 360$ nm). The insets show the residuals of the fits.

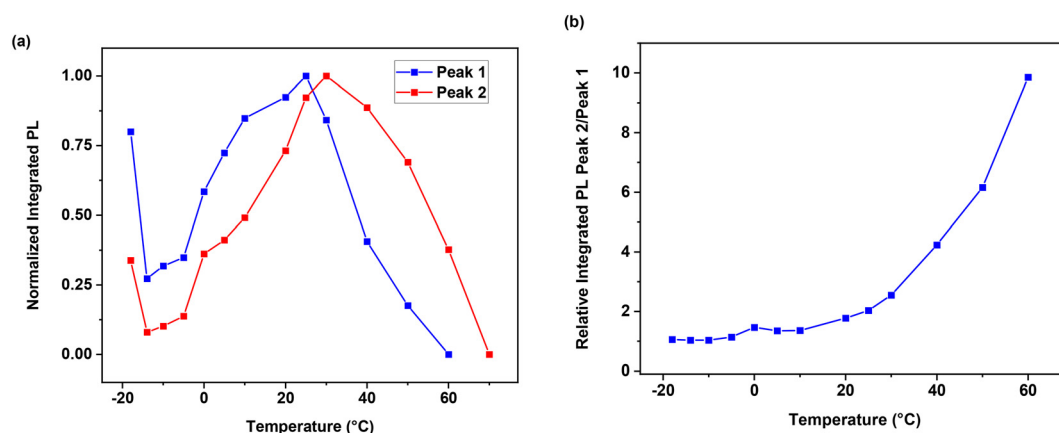


Fig. 5 For $(\text{C}_{16}\text{H}_{33}\text{NH}_3)_2\text{PbI}_4$, (a) the variation of the normalized integrated PL peak intensity is temperature dependent between -18 and 70 °C, and (b) the relative intensity of Peak 2 to Peak 1 increases.

longest time component, and the data are best fit by a bi-exponential decay process ($\tau_1 = 39$ ns and $\tau_2 = 394$ ns) that is heavily weighted towards the shortest time constant ($A_1 = 0.85$ vs. $A_2 = 0.15$) as seen in Fig. 4b. We have associated the single PL peak at -196 °C with the RT phase (484 nm emission). At this temperature, we did not observe the HT phases. By decreasing the temperature, shorter lifetimes are observed, which corresponds with more excitonic character and less of a trap-state or triplet character.

For $(\text{C}_{16}\text{H}_{33}\text{NH}_3)_2\text{PbI}_4$, the integrated intensities of Peak 1 and Peak 2 are identical for temperatures between -18 °C and -5 °C (Fig. 5b and S5c†). Upon warming the sample to 0 °C, the population of Peak 2 ($\lambda_{\text{max}} = 514$ nm) begins to dominate and a bathochromic shift to 525 nm is present until 30 °C. Unlike $(\text{C}_{18}\text{H}_{37}\text{NH}_3)_2\text{PbI}_4$, for $(\text{C}_{16}\text{H}_{33}\text{NH}_3)_2\text{PbI}_4$, the intensity of both peaks increased from -15 °C and reached to its maxima at +25 °C for Peak 1 and at +30 °C for Peak 2. After that, the intensity of both bands decreases until they were below the detection limit at 70 °C for Peak 1 and 80 °C for Peak 2 and the third phase (HT, monoclinic) which is poorly

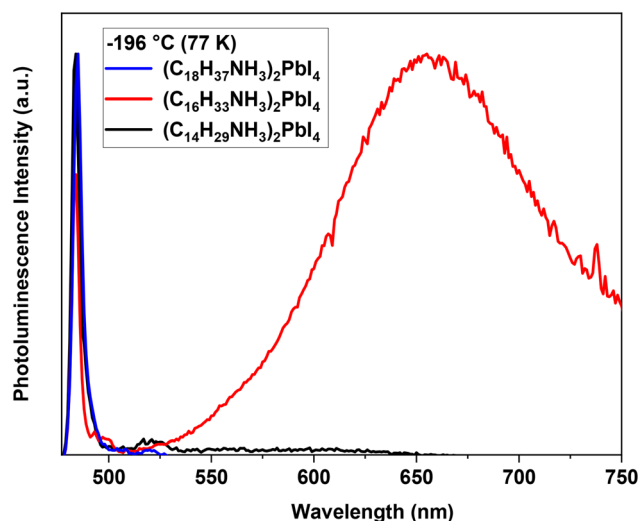


Fig. 6 Normalized photoluminescence spectra of the three 2D perovskite powders at -196 °C.



emissive appeared higher than 80 °C. According to XRD, an increase in the temperature results in a more symmetrical geometry of the inorganic planes and the average bond length decreasing slightly in the new monoclinic system compared to that in the orthorhombic system (RT phase).¹⁸

At −196 °C, there is one narrow peak positioned at 483 nm and a broad and intense emission band at 625 nm. The sharp, higher energy peak corresponds to the RT phase, which appears as another phase transition below −20 °C. The lower energy band was not observed for (C₁₈H₃₇NH₃)₂PbI₄ or (C₁₄H₂₉NH₃)₂PbI₄ and may indicate that internal energy transfer is more important for (C₁₆H₃₃NH₃)₂PbI₄ than in the other compounds (Fig. 6). The results are consistent with the observed lower quantum yield for (C₁₆H₃₃NH₃)₂PbI₄ when compared with those of (C₁₈H₃₇NH₃)₂PbI₄ and (C₁₄H₂₉NH₃)₂PbI₄ (Table 1 and Fig. S8†).

The behavior of (C₁₄H₂₉NH₃)₂PbI₄ is similar to that of (C₁₈H₃₇NH₃)₂PbI₄ and in both compounds, the integrated PL intensity dropped precipitously at −10 °C and continued for both PL peaks until they were below the detection limit at 65 and 75 for Peak 1 and Peak 2, respectively (Fig. S6c†). At −196 °C, only the first narrow PL band is observed for (C₁₄H₂₉NH₃)₂PbI₄, which is associated with the LT phase (Fig. 6). The decay constants and pre-exponential factors for (C₁₄H₂₉NH₃)₂PbI₄ were similar at room temperature and low temperature, which may suggest that there is greater similarity between the two phases (LT and RT) as compared to (C₁₈H₃₇NH₃)₂PbI₄ (Fig. S7†).

4. Conclusion

In summary, temperature-dependent steady-state photoluminescence (PL) and temperature-dependent time-resolved photoluminescence (TRPL) spectroscopy have been successfully applied to study the multiple phase transitions and excited-state decay in the temperature range of −18 to 90 °C and at −196 °C. The observed reversible temperature response confirms the reversibility of the phase transition in the studied compounds. Our observations show that the color of the sample transitions from yellow to orange at the phase transition temperature from the RT to HT phase and the emission changes from blue to green from low to room temperature (RT phase) due to different excited states. Furthermore, it seems that the longer the alkyl chain in the organic chain is, the higher the temperature of the phase transition. This involves enhanced conformational and dynamic disorder (or melting) of the organic chain, and an increase in the perovskite symmetry. Furthermore, the decay constants for all compounds are very close in value and showed multi-component constants confirming the contribution of the same fragments in all of them (inorganic part). However, a longer PL decay is not observed at a low temperature (−196 °C) for (C₁₈H₃₇NH₃)₂PbI₄ and (C₁₆H₃₃NH₃)₂PbI₄ which is evidence for more changes in the inorganic part of the compounds between LT and RT phases. Further investigations in the temperature range from

−196 to −18 °C by powder X-ray diffraction could provide more information on the structures and conformational alteration, especially for the LT phase and the exact temperature of phase transition.

Conflicts of interest

There are no conflicts to declare.

Acknowledgements

We gratefully acknowledge the Swedish Energy Agency for financial support (Grant number: 49278-1). Further support for this research was possible due to the generous contributions of the Swedish government through the strategic research area "StandUP for ENERGY". We would like to thank Dr Veronica Paterlini for helping us with the time-resolved measurements at Stockholm University and KTH's Department of Chemistry for supplying the caffeine required for completing this work. JG would like to thank Brian David Gardner and Rachael Elizabeth Gardner for their insightful conversations and vigorous debates.

References

- 1 E. Elahi, G. Dastgeer, A. S. Siddiqui, S. A. Patil, M. W. Iqbal and P. R. Sharma, A review on two-dimensional (2D) perovskite material-based solar cells to enhance the power conversion efficiency, *Dalton Trans.*, 2022, **51**, 797–816.
- 2 B. P. Kore, W. Zhang, B. W. Hoogendoorn, M. Safdari and J. M. Gardner, Moisture tolerant solar cells by encapsulating 3D perovskite with long-chain alkylammonium cation-based 2D perovskite, *Commun. Mater.*, 2021, **2**, 100.
- 3 A. Lemmerer, Thermochromic Phase Transitions of Long Odd-Chained Inorganic–Organic Layered Perovskite-Type Hybrids [(C_nH_{2n+1}NH₃)₂PbI₄], n = 11, 13, and 15, *Inorg. Chem.*, 2022, **61**, 6353–6366.
- 4 B. P. Kore, M. Jamshidi and J. M. Gardner, The impact of moisture on the stability and degradation of perovskites in solar cells, *Mater. Adv.*, 2024, **5**, 2200–2217.
- 5 M. M. Abdelkader and W. M. Gamal, Characterization and coordination of intercalation - Non-intercalation phase transition in a new hybrid halide perovskite (n-C₁₆H₃₃NH₃)₂ZnCl₄, *Solid State Sci.*, 2016, **61**, 173–184.
- 6 B. Traore, L. Pedesseau, L. Assam, X. Che, J.-C. Blancon, H. Tsai, W. Nie, C. C. Stoumpos, M. G. Kanatzidis, S. Tretiak, A. D. Mohite, J. Even, M. Kepenekian and C. Katan, Composite Nature of Layered Hybrid Perovskites: Assessment on Quantum and Dielectric Confinements and Band Alignment, *ACS Nano*, 2018, **12**, 3321–3332.
- 7 C. M. Mauck and W. A. Tisdale, Excitons in 2D Organic–Inorganic Halide Perovskites, *Trends Chem.*, 2019, **1**, 380–393.



- 8 J. C. Blancon, A. V. Stier, H. Tsai, W. Nie, C. C. Stoumpos, B. Traoré, L. Pedesseau, M. Kepenekian, F. Katsutani, G. T. Noe, J. Kono, S. Tretiak, S. A. Crooker, C. Katan, M. G. Kanatzidis, J. J. Crochet, J. Even and A. D. Mohite, Scaling law for excitons in 2D perovskite quantum wells, *Nat. Commun.*, 2018, **9**, 2254.
- 9 D. B. Straus and C. R. Kagan, Electrons, Excitons, and Phonons in Two-Dimensional Hybrid Perovskites: Connecting Structural, Optical, and Electronic Properties, *J. Phys. Chem. Lett.*, 2018, **9**, 1434–1447.
- 10 L. Mao, C. C. Stoumpos and M. G. Kanatzidis, Two-Dimensional Hybrid Halide Perovskites: Principles and Promises, *J. Am. Chem. Soc.*, 2019, **141**, 1171–1190.
- 11 F. Zhang, H. Lu, J. Tong, J. J. Berry, M. C. Beard and K. Zhu, Advances in two-dimensional organic–inorganic hybrid perovskites, *Energy Environ. Sci.*, 2020, **13**, 1154–1186.
- 12 A. H. Proppe, M. Wei, B. Chen, R. Quintero-Bermudez, S. O. Kelley and E. H. Sargent, Photochemically Cross-Linked Quantum Well Ligands for 2D/3D Perovskite Photovoltaics with Improved Photovoltage and Stability, *J. Am. Chem. Soc.*, 2019, **141**, 14180–14189.
- 13 D. H. Kim, C. P. Muzzillo, J. Tong, A. F. Palmstrom, B. W. Larson, C. Choi, S. P. Harvey, S. Glynn, J. B. Whitaker, F. Zhang, Z. Li, H. Lu, M. F. A. M. van Hest, J. J. Berry, L. M. Mansfield, Y. Huang, Y. Yan and K. Zhu, Bimolecular Additives Improve Wide-Band-Gap Perovskites for Efficient Tandem Solar Cells with CIGS, *Joule*, 2019, **3**, 1734–1745.
- 14 K. Zheng, Y. Chen, Y. Sun, J. Chen, P. Chábera, R. Schaller, M. J. Al-Marri, S. E. Canton, Z. Liang and T. Pullerits, Interphase charge and energy transfer in Ruddlesden–Popper 2D perovskites: critical role of the spacing cations, *J. Mater. Chem. A*, 2018, **6**, 6244–6250.
- 15 A. H. Proppe, M. H. Elkins, O. Voznyy, R. D. Pensack, F. Zapata, L. V. Besteiro, L. N. Quan, R. Quintero-Bermudez, P. Todorovic, S. O. Kelley, A. O. Govorov, S. K. Gray, I. Infante, E. H. Sargent and G. D. Scholes, Spectrally Resolved Ultrafast Exciton Transfer in Mixed Perovskite Quantum Wells, *J. Phys. Chem. Lett.*, 2019, **10**, 419–426.
- 16 M. Safdari, P. H. Svensson, M. T. Hoang, I. Oh, L. Kloo and J. M. Gardner, Layered 2D alkyldiammonium lead iodide perovskites: synthesis, characterization, and use in solar cells, *J. Mater. Chem. A*, 2016, **4**, 15638–15646.
- 17 F. Li, Y. Xie, Y. Hu, M. Long, Y. Zhang, J. Xu, M. Qin, X. Lu and M. Liu, Effects of Alkyl Chain Length on Crystal Growth and Oxidation Process of Two-Dimensional Tin Halide Perovskites, *ACS Energy Lett.*, 2020, **5**, 1422–1429.
- 18 D. G. Billing and A. Lemmerer, Synthesis, characterization and phase transitions of the inorganic–organic layered perovskite-type hybrids [(CnH_{2n}+1NH₃)₂PbI₄] (n = 12, 14, 16 and 18), *New J. Chem.*, 2008, **32**, 1736–1746.
- 19 D. Spirito, Y. Asensio, L. E. Hueso and B. Martín-García, Raman spectroscopy in layered hybrid organic–inorganic metal halide perovskites, *Journal of Physics: Materials*, 2022, **5**, 034004.
- 20 J. M. Hoffman, C. D. Malliakas, S. Sidhik, I. Hadar, R. McClain, A. D. Mohite and M. G. Kanatzidis, Long periodic ripple in a 2D hybrid halide perovskite structure using branched organic spacers, *Chem. Sci.*, 2020, **11**, 12139–12148.
- 21 K. Fedoruk, D. Drozdowski, M. Maczka, J. K. Zareba, D. Stefańska, A. Gabor and A. Sieradzki, [Methylhydrazinium]₂PbCl₄, a Two-Dimensional Perovskite with Polar and Modulated Phases, *Inorg. Chem.*, 2022, **61**, 15520–15531.
- 22 M. Zhang, M. Li, X. You, Z. Wei, W. Rao, L. Wang and H. Cai, A fluorine and chlorine substituted 2D lead bromide perovskite with high phase transition temperature, *J. Solid State Chem.*, 2021, **302**, 122409.
- 23 Q. Gao, J. Qi, K. Chen, M. Xia, Y. Hu, A. Mei and H. Han, Halide Perovskite Crystallization Processes and Methods in Nanocrystals, Single Crystals, and Thin Films, *Adv. Mater.*, 2022, **34**, 2200720.
- 24 W. Paritmongkol, N. S. Dahod, A. Stollmann, N. Mao, C. Settens, S.-L. Zheng and W. A. Tisdale, Synthetic Variation and Structural Trends in Layered Two-Dimensional Alkylammonium Lead Halide Perovskites, *Chem. Mater.*, 2019, **31**, 5592–5607.
- 25 A. Lemmerer and D. G. Billing, Synthesis, characterization and phase transitions of the inorganic–organic layered perovskite-type hybrids [(CnH_{2n}+1NH₃)₂PbI₄], n = 7, 8, 9 and 10, *Dalton Trans.*, 2012, **41**, 1146–1157.
- 26 C. C. Stoumpos, D. H. Cao, D. J. Clark, J. Young, J. M. Rondinelli, J. I. Jang, J. T. Hupp and M. G. Kanatzidis, Ruddlesden–Popper Hybrid Lead Iodide Perovskite 2D Homologous Semiconductors, *Chem. Mater.*, 2016, **28**, 2852–2867.
- 27 N. V. Venkataraman, S. Bhagyalakshmi, S. Vasudevan and R. Seshadri, Conformation and orientation of alkyl chains in the layered organic–inorganic hybrids: (CnH_{2n}+1NH₃)₂PbI₄ (n = 12, 16, 18), *Phys. Chem. Chem. Phys.*, 2002, **4**, 4533–4538.
- 28 B. P. Kore and J. M. Gardner, Water-resistant 2D lead(II) iodide perovskites: correlation between optical properties and phase transitions, *Mater. Adv.*, 2020, **1**, 2395–2400.
- 29 N. V. Venkataraman, S. Barman, S. Vasudevan and R. Seshadri, Structural analysis of alkyl chain conformation in the layered organic–inorganic hybrids (CnH_{2n}+1NH₃)₂PbI₄ (n=12,16,18) by IR spectroscopy, *Chem. Phys. Lett.*, 2002, **358**, 139–143.
- 30 K.-H. Wang, L.-C. Li, M. Shellaiah and K. W. Sun, Structural and Photophysical Properties of Methylammonium Lead Tribromide (MAPbBr₃) Single Crystals, *Sci. Rep.*, 2017, **7**, 13643.
- 31 D. W. deQuilettes, W. Zhang, V. M. Burlakov, D. J. Graham, T. Leijtens, A. Osherov, V. Bulović, H. J. Snaith, D. S. Ginger and S. D. Stranks, Photo-induced halide redistribution in organic–inorganic perovskite films, *Nat. Commun.*, 2016, **7**, 11683.



- 32 A. Oshero, E. M. Hutter, K. Galkowski, R. Brenes, D. K. Maude, R. J. Nicholas, P. Plochocka, V. Bulović, T. J. Savenije and S. D. Stranks, The Impact of Phase Retention on the Structural and Optoelectronic Properties of Metal Halide Perovskites, *Adv. Mater.*, 2016, **28**, 10757–10763.
- 33 O. Vukovic, G. Folpini, E. L. Wong, L. Leoncino, G. Terraneo, M. D. Albaqami, A. Petrozza and D. Cortecchia, Structural effects on the luminescence properties of CsPbI₃ nanocrystals, *Nanoscale*, 2023, **15**, 5712–5719.
- 34 T. Sheikh, A. Shinde, S. Mahamuni and A. Nag, Possible Dual Bandgap in (C₄H₉NH₃)₂PbI₄ 2D Layered Perovskite: Single-Crystal and Exfoliated Few-Layer, *ACS Energy Lett.*, 2018, **3**, 2940–2946.
- 35 Y. Han, Y. Li, Y. Wang, G. Cao, S. Yue, L. Zhang, B.-B. Cui and Q. Chen, From Distortion to Disconnection: Linear Alkyl Diammonium Cations Tune Structure and Photoluminescence of Lead Bromide Perovskites, *Adv. Opt. Mater.*, 2020, **8**, 1902051.
- 36 C.-W. Lin, F. Liu, T.-Y. Chen, K.-H. Lee, C.-K. Chang, Y. He, T. L. Leung, A. M. C. Ng, C.-H. Hsu, J. Popović, A. Djurišić and H. Ahn, Structure-Dependent Photoluminescence in Low-Dimensional Ethylammonium, Propylammonium, and Butylammonium Lead Iodide Perovskites, *ACS Appl. Mater. Interfaces*, 2020, **12**, 5008–5016.
- 37 V. V. Nawale, T. Sheikh and A. Nag, Dual Excitonic Emission in Hybrid 2D Layered Tin Iodide Perovskites, *J. Phys. Chem. C*, 2020, **124**, 21129–21136.
- 38 D. Cortecchia, S. Neutzner, A. R. S. Kandada, E. Mosconi, D. Meggiolaro, F. De Angelis, C. Soci and A. Petrozza, Broadband Emission in Two-Dimensional Hybrid Perovskites: The Role of Structural Deformation, *J. Am. Chem. Soc.*, 2017, **139**, 39–42.
- 39 M. Jamshidi, S. R. Barzegar-Kiadehi, M. G. Haghighi and B. Notash, Dual-Emissive Bis(diphenylphosphino)amine Platinum Complexes: Structural, Reactivity, Photophysical, and Theoretical Investigations, *Organometallics*, 2020, **39**, 3099–3111.
- 40 R. F. Moral, J. C. Germino, L. G. Bonato, D. B. Almeida, E. M. Therézio, T. D. Z. Atvars, S. D. Stranks, R. A. Nome and A. F. Nogueira, Influence of the Vibrational Modes from the Organic Moieties in 2D Lead Halides on Excitonic Recombination and Phase Transition, *Adv. Opt. Mater.*, 2020, **8**, 2001431.
- 41 B. Dryzhakov, B. J. Lawrie, J. Z. Celio, M. Wang, M. Koehler and B. Hu, Dual Emission Bands of a 2D Perovskite Single Crystal with Charge Transfer State Characteristics, *ACS Nano*, 2023, **17**, 12200–12207.
- 42 K. Pradeesh, J. J. Baumberg and G. V. Prakash, Temperature-induced exciton switching in long alkyl chain based inorganic-organic hybrids, *J. Appl. Phys.*, 2012, **111**, 013511.
- 43 M. Bruzzi, F. Gabelloni, N. Calisi, S. Caporali and A. Vinattieri, Defective States in Micro-Crystalline CsPbBr₃ and Their Role on Photoconductivity, *Nanomaterials*, 2019, **9**, 177.
- 44 T. Sheikh, A. Shinde, S. Mahamuni and A. Nag, Dual excitonic emissions and structural phase transition of octylammonium lead iodide 2D layered perovskite single crystal, *Mater. Res. Express*, 2019, **6**, 124002.
- 45 Laxmi and D. Kabra, Origin of Contrasting Emission Spectrum of Bromide versus Iodide Layered Perovskite Semiconductors, *J. Phys. Chem. Lett.*, 2022, **13**, 2737–2743.
- 46 B. B. Chen, S. Wang, S. W. Jiang, Z. G. Yu, X. G. Wan, H. F. Ding and D. Wu, The role of heavy metal ions on spin transport in organic semiconductors, *New J. Phys.*, 2015, **17**, 013004.

